This is a peer-reviewed, accepted author manuscript of the following article: Javadi, Y., Najafabadi, M. A., & Akhlaghi, M. (2012). Residual stress evaluation in dissimilar welded joints using finite element simulation and the L CR ultrasonic wave. *Russian Journal of Nondestructive Testing*, *48*(9), 541-552. https://doi.org/10.1134/S1061830912090033

# Residual stress evaluation in dissimilar welded joints using finite element simulation and the $L_{CR}$ ultrasonic wave

Yashar Javadi, Mehdi Ahmadi Najafabadi[1], Mehdi Akhlaghi

*Department of Mechanical Engineering, Amirkabir University of Technology, 424 Hafez Ave., Tehran, Iran.*

**Abstract**

Subsurface stresses in welded structures increase the likelihood of fatigue cracks and environmental induced material degradation. The ability to evaluate stresses at the surface as well as in the interior of welded structural members would substantially increase the accuracy of structure life estimation. The longitudinal critically refracted ( $L_{CR}$ ) wave is a bulk longitudinal mode that travels within an effective depth underneath the surface. It may be used to detect in-plane subsurface stresses in the structures. This paper presents a three dimensional thermo-mechanical analysis to evaluate welding residual stresses in dissimilar plate-plate joint of AISI stainless steel 304 and Carbon Steel A106-B type. After finite element simulation, the residual stresses were evaluated by $L_{CR}$ ultrasonic waves. Finally the results of two methods were compared and verified by hole-drilling method. This paper introduces a combination of "Finite Element Welding Simulation" and "Ultrasonic Stress Measurement using the $L_{CR}$ Wave" which is called as "$FEL_{CR}$". The capabilities of $FEL_{CR}$ in residual stress measurement are confirmed here. And also this paper evaluates residual stresses of dissimilar welded joints by $L_{CR}$ ultrasonic waves. It has been shown that predicted residual stress from three dimensional FE analyses is in reasonable agreement with measured residual stress from $L_{CR}$ method and also the results of both are verified with hole-drilling experimental measurements.

***Keywords:*** *Finite Element Welding Simulation; Ultrasonic Stress Measurement; Acoustoelastic Effect; Welding Residual Stress;* $L_{CR}$ *;* $FEL_{CR}$ *; Hole-Drilling Measurement; Dissimilar Welded Joint.*

## 1- Introduction

Residual stresses are present in materials without any external pressure, and generally result from deformation heterogeneities appearing in the material [1]. They play an important role in the strength and service life of structures. Welding is an assembly process often used in the mechanical industries, especially in the pressure vessel industry. According to the process and temperatures reached during this operation, harmful thermo-mechanical stresses may appear in the welded joint. To optimize the structures' design and control their mechanical strength in service, it is very important to determine the residual stress levels with a non-destructive method. The high industry request for the stress evaluation

[1] Corresponding author, Tel.:+98 21 6454 3431; fax:+98 21 66419736
Email addresses: ahmadin@aut.ac.ir (M. Ahmadi Najafabadi)

techniques encouraged development of several methods like X-ray diffraction, incremental hole drilling, and more recently the ultrasonic waves and the Barkhausen noise methods. Many studies clearly showed that there is no universal or absolute method that gives complete satisfaction in the in-situ non-destructive stress monitoring of the mechanical components. Many parameters such as material, geometry, surface quality, cost, and accuracy of the measurement, etc., must be taken into account in choosing an adequate method.

### *1-1- Ultrasonic method*

The ultrasonic method was chosen for stress measurement because it is non-destructive, easy to use, and relatively inexpensive. However, it is rather sensitive to the microstructure effects (grains size [2, 3, 4], carbon rate [5, 6], texture [7, 8, 9, 10], and structure [11, 12, 13]) and to the operating conditions (temperature [14, 15], coupling [16, 17], etc.). The ultrasonic evaluation of the residual stresses requires separation between the microstructure and the acoustoelastic effects.

### *1-2- Welding Simulation*

The extent of deformations and residual stresses in welded components depends on several factors such as geometrical size, welding parameters, welding sequence and applied structural boundary conditions. Finite element (FE) simulation has become a popular tool for the prediction of welding distortions and residual stresses. Earlier studies of welding accounted for the non-linearities due to temperature dependent material properties and plastic deformations [18, 19, 20]. The majority of those analyses were limited to two-dimensions on the plane perpendicular to the welding direction. Good correlations have been observed between the numerical predictions and experimental results [21, 22, 23, 24].

## 2- Theoretical Background

### *2-1- Acoustoelastic Effect*

Within the elastic limit, the ultrasonic stress evaluating method relies on a linear relationship between the stress and the velocity or the travel time change, i.e. the acoustoelastic effect [25, 26]. The $L_{CR}$ method uses a special longitudinal bulk wave mode, as shown in Fig.1, which travels parallel to the surface, particularly propagating beneath the surface at a certain depth. The $L_{CR}$ waves are also called surface skimming longitudinal waves (SSLW) by other authors. Brekhovskii [27], Basatskaya and Ermolov [28], Junghans and Bray [29], Langenberg et al. [30] had some detailed discussions on the characteristics of the critically refracted waves.

Ultrasonic stress measurement techniques are based on the relationship of wave speed in various directions with stress. Fig. 2 shows elements of a bar under tension where the wave propagates in three perpendicular directions.

The first index in the velocities represents the propagation direction for the wave and the second represents the direction of the movement of the particles. In Fig. 2a the wave propagates parallel to the load and $V_{11}$ represents the velocity of the particles in the same direction (longitudinal wave), meanwhile $V_{12}$ and $V_{13}$ represents the velocity in a perpendicular plane (shear waves).

In Fig. 2b and c the waves propagating in the other directions and the velocities symbols are also shown. The $V_{22}$ velocity is for longitudinal waves propagating perpendicular to the stress field. The sensitivity of these waves to the strain has been established by Egle and Bray [25] in tensile and compressive load tests for a bar of pearlitic (rail) steel. The waves with particle motion in the direction of the stress fields showed the greatest sensitivity to stress, and those with particle motions

perpendicular to the stress field showed the least. The most significant variation in travel time with the strain was found for longitudinal waves, followed by the shear waves when the particles vibrate in the direction of the load. The other waves do not show significant sensitivity to the deformation. The speeds of the longitudinal plane waves traveling parallel to load can be related to the strain (α) by the following expressions:

$$\rho_0 V_{11}^{\ 2} = \lambda + 2\mu + (2l + \lambda)\theta + (4m + 4\lambda + 10\mu)\alpha_1 \quad (1)$$

where $\rho_0$ is the initial density; $V_{11}$ is the velocity of waves in the direction 1 with particle displacement in the direction 1; λ, μ the second order elastic constants (Lame's constants); *l*, *m*, *n* are the third order elastic constants; $\theta = \alpha_1 + \alpha_2 + \alpha_3$ which $\alpha_1$, $\alpha_2$ and $\alpha_3$ are components of the homogeneous triaxial principal strains. For a state of uniaxial stress, $\alpha_1 = \varepsilon$, $\alpha_2 = \alpha_3 = -\upsilon \times \varepsilon$, where ε is the strain in the direction 1 and υ is the Poisson's ratio. Using these values, Eq. (1) becomes:

$$\rho_0 V_{11}^{\ 2} = \lambda + 2\mu + [4(\lambda + 2\mu) + 2(\mu + 2m) + \nu\mu(1 + \frac{2\lambda}{\mu})].\varepsilon \quad (2)$$

The relative sensitivity is the variation of the velocity with the strain and can be calculated by Eq. (3). In this equation, $L_{11}$ is the dimensionless acoustoelastic constant for $L_{CR}$ waves.

$$\frac{dV_{11}/V_{11}}{d\varepsilon} = 2 + \frac{(\mu + 2m) + \nu\mu(1 + 2l/\lambda)}{\lambda + 2\mu} = L_{11} \quad (3)$$

The values for acoustoelastic constants for other directions can be obtained in the same way. The variation in the $v_{11}$ velocity, controlled by the coefficient $L_{11}$, is much greater than the other ones, indicating that these waves are the best candidates to be used in the stress evaluation. Stress can be calculated by the one-dimensional application of the stress–strain relations in elastic solids. Eq. (3) can be rearranged to give the stress variation in terms time-of-flight ($dt/t_0$), as shown in the Eq. (4), where $t_0$ is the time for the wave to go through a stress free path in the material being investigated.

$$d\sigma = \frac{E(dV_{11}/V_{11})}{L_{11}} = \frac{E}{L_{11}t_0}dt \quad (4)$$

where dσ is the stress variation (MPa) and *E* is the elasticity modulus (MPa). The same equation can be used for the other directions of the waves, provided the value of the acoustoelastic coefficient *L* is changed. For a fixed probe distance, the travel time of the longitudinal wave decreases in a compressive stress field and increases in a tensile field. The acoustoelastic constant (*L*) functionally links the stress and the velocity or travel time change.

### *2-2- Finite Element Welding Simulation*

#### *2-2-1- Modeling of physical phenomena*

Numerical simulation of residual stresses and distortions due to welding need to accurately take account of the interactions between heat transfer, metallurgical transformations and mechanical fields. The phenomena involved in the heat input such as arc, material interactions as well as fluid dynamics in the weld pool are not accurately described. From the thermo-mechanical point of view, the heat input can be seen as a volumetric or surfaced energy distribution, and the fluid flow effect, which leads to homogenize the temperature in the molten area, can be simply taken into account by increasing the thermal conductivity over the fusion temperature. As no metallurgical transformation occurs in the 304 stainless steel considered in this paper, no detailed modeling of the melting is considered here. Of course this will be caused to some error in predicting the residual stresses in the carbon steel side of the plates studied here. Heat transfers in solids are described by the heat equation:

$$\rho \frac{dH}{dt} - div(\lambda gradT) - Q = 0 \quad (5)$$

$$\lambda gradT.n = q(T,t) \quad \text{on} \quad \partial\Omega_q \quad (6)$$

$$T = T_p(t) \quad \text{on} \quad \partial\Omega_t \quad (7)$$

Where ρ, H, λ and T are density, enthalpy, thermal conductivity and temperature, respectively. In Eq. (5), Q represents an internal heat source. In Eq. (6), n is the outward normal vector of domain δΩ and q the heat flux density that can depend on temperature and time to model convective heat exchanges on the surface. $T_p$ represents a prescribed temperature. The heat input is represented by an internal heat source. In the present study, the double ellipsoid heat source configuration proposed by Goldak et al. [32] is used, as shown in Fig. 3. As it is seen, the front half of the heat source is the quadrant of one ellipsoidal source, and the rear half is the quadrant of another ellipsoid. In this model, the fractions of ff and fr of the heat deposited in the front and rear quadrants are needed, where ff+fr=2. The power density distribution inside the front quadrant is:

$$q_f(x,y,z) = \frac{6\sqrt{3} f_f Q}{a_f bc\pi^{3/2}} e^{(-3x^2/a_f^2)} e^{(-3y^2/b^2)} e^{(-3z^2/c^2)} \quad (8)$$

Similarly, for the rear quadrant of the source the power density distribution inside the ellipsoid becomes:

$$q_r(x,y,z) = \frac{6\sqrt{3} f_r Q}{a_r bc\pi^{3/2}} e^{(-3x^2/a_r^2)} e^{(-3y^2/b^2)} e^{(-3z^2/c^2)} \quad (9)$$

Physically these parameters are the radial dimensions of the molten zone in front, behind, to the side, and underneath the arc. If the cross-section of the molten zone is known from the experiment, these data may be used to fix the heat source dimensions. If cross-sectional dimensions are not available, the experience data given by Goldak et al. [32] suggest that it is reasonable to take the distance in front of the heat source equal to one-half the weld width and the distance behind the heat source equal to twice the width. These suggestions are used in this paper. The internal heating due to the plastic dissipation can be neglected considering the small transformation rates generated by a welding operation.

The mechanical analysis is based on the usual equations describing the static equilibrium. As the plastic dissipation is neglected in the thermal analysis, thermal and mechanical analyses can be treated separately. Thus, the mechanical calculation is achieved using the temperature fields computed previously by the thermal analysis. The materials are supposed to follow an elastic–plastic behavior with isotropic hardening. The material parameters Young's modulus, Poisson's ratio, yield stress, strain hardening and heat expansion coefficient are temperature dependent.

### *2-2-2- Material modeling*

Material modeling has always been a critical issue in the simulation of welding because of the scarcity of material data at elevated temperatures. Some simplifications and approximations are usually introduced to cope with this problem. These simplifications are necessary due to both lack of data and numerical problems when trying to model the actual high-temperature behavior of the material [33]. The material properties for AISI 304 stainless steel and A106 carbon steel are shown in Fig. 4 and Fig. 5 respectively. These data are taken from Lindgren [34] and P. Chang [35]. In these figures, α is coefficient of linear *thermal expansion*, c is specific Heat, E is elastic modulus, k is thermal conductivity and σy is yield stress. The filler metals are determine with help to Schaeffler Diagram [36].

### *2-2-3- Finite element modeling*

The problem is formulated as a sequentially coupled thermal stress analysis. First, a non-linear thermal analysis is performed to calculate the temperature history of the whole domain. Then, the results of the thermal analysis are applied as a thermal body load in a non-linear structural analysis to determine distortions. The finite element models for both thermal and structural analysis are the same. The general-purposed FE program ANSYS is used for the analyses. During the analysis a full Newton-Raphson iterative solution technique with direct sparse matrix solver is employed for obtaining a solution. During the thermal analysis, the temperature and the temperature dependent material properties change very rapidly. Thus, a full Newton-Raphson technique with using modified material properties is believed to give more accurate results. A conventional element technique named 'element birth and death' Lindgren [37] is used for modelling of the deposited weld. A complete FE model is generated in the start of the analysis. However, all elements representing the deposited weld except elements for the tack welds are deactivated by assigning them a very low stiffness. During the thermal analysis, all the nodes of deactivated elements (excluding those shared with the base metal) are also fixed at room temperature till the birth of the respective element. Deactivated elements are reactivated sequentially when they come under the influence of the welding torch. Linear elements are preferred than higher-order elements in non-linear problems of this type [38]. Here, eight-noded-brick elements with linear shape functions are used in the FE modeling. The basic FE model of plates is shown in Fig. 6.

## 3- Experimental Procedures

### *3-1- Sample Description*

The materials tested (A106-B and A240-TP304) are commonly used for pressure vessel applications. Four passes butt-weld joint geometry with 4mm root gap was used. Two 450*200*8 mm normalized A106-B and A240-TP304 rolled plates were welded in V-groove (60° included angle), root pass by the tungsten inert gas (TIG) and the other weld-passes by shielded metal arc welding (SMAW) process. Two calibration samples were extracted from A106-B and A240-TP304 base metal to determine acoustoelastic constants.

### *3-2- Measurement Device*

The measurement device, shown in Fig. 7, includes an Ultrasonic box with integrated pulser and receiver (OPBOX - USB 2.0), computer and two normal transducers assembled on two wedges.
The nominal frequency and diameter of the piezoelectric elements are 2 MHz and 24 mm, respectively. Transducers were screwed on the PMMA plastic wedges. OPBOX - USB 2.0 is a 100Mhz ultrasonic testing device which has a synchronization between the pulser signal and the internal clock, that controls the A/D converter. This allows very precise measurements of the time of flight – better than 1ns. Post trigger (delay) time is software programmable in the range of 0 - 255us with a resolution of 1us and has stability within the range of 1ns. 1ns would correspond to a clock frequency of 1GHz which is much higher than the actual frequency used.

### *3-3- Evaluation of the Calibration Constants*

To evaluate the calibration constants (acoustoelastic constant, free stress time-of-flight), the calibration samples were taken in the direction parallel to the weld in order to avoid the texture influence (see Fig.8). This direction also corresponds to that of the measured stress. Two separated samples (A106-B and A240-TP304) were obtained from PM (parent metal) region of plates. To evaluate the residual

stress from equation4, the value $t_0$ is measured directly from the stress-free samples and the acoustoelastic constant ($L_{11}$) is deduced experimentally from a uniaxial tensile test associated with an ultrasonic measurement (Fig.8). Acoustoelastic constant represents the slope of the relative variation curve of the time-of-flight and the applied stress. (as shown in Fig.9 and Fig.10)

## 4- Results and Discussion

### *4-1- Ultrasonic Determination of Residual Stresses*

In this study, the ultrasonic measurement concerns the subsurface residual stresses. The measurements were parallel to the weld axis. The values of the residual stresses relating to each weld zone were calculated from the equations (1-4) and the results are shown in Fig. 11.

### *4-2- Finite Element Determination of Residual Stresses*

The FE model was run for 4 weld-passes process and its residual stresses were calculated for both side of the weld centerline. The FE results are shown in Fig. 12.

### *4-3- Hole-Drilling Determination of Residual Stresses*

For the hole-drilling method, a strain gauge rosette was bonded on each weld zone and drilling was performed incrementally (step by step) until 2 mm. There was no significant stress gradient encountered between the successive depths, this is why the measurements were integrated on the total depth of 2 mm.

### *4-4- Comparison between the Ultrasonic, Finite Element and Hole-drilling method results*

Comparison between the ultrasonic, finite element and hole-drilling method results was performed in order to validate our measurements. The results are shown in Fig. 13.
From Fig. 13 it can be concluded that:

1. There is a good correlation between Finite Element and Hole-Drilling results.
2. Finite Element results were in reasonable agreement with Ultrasonic measurements in the weld zone and parent-metal. But ultrasonic method had a wrong prediction of residual stresses in the HAZ (heat affected zone) because of complicated microstructure of this region. In this zone, the ultrasonic overestimation of the residual stresses is due to the microstructure effect, since PM calibration constants were used instead of the HAZ constant. To get a good results in the HAZ, reproducing the microstructure of this zone using a specific heat treatment mentioned in Qozam et al.[39] is required.
3. Combining finite element with ultrasonic stress measurement ($FEL_{CR}$) in the welding process has studied here. Advantages of this combination are:
    a. Predicting exact dimensions of welding regions (Parent-metal, HAZ and Weld-zone) by finite element and use it to exactly determine tensile strength samples for evaluating accostoelastic constants.
    b. Have a good knowledge of bulk stresses by finite element analysis and use it to verify $L_{CR}$ capability of bulk stress measurement.
    c. Research documentations in finite element is more than ultrasonic stress measurement so it can be said that FE is more reliable than ultrasonic in stress measurement and it can be supplement of ultrasonic especially in the absent of the other stress measurement methods.

## 5- Conclusion

This paper confirms the potential of the $FEL_{CR}$ (which has been introduced here) to accurately evaluate the welding residual stresses. $FEL_{CR}$ can be developed and will work better if:

1- Tensile strength samples are extracted from all of the welding zones.
2- Microstructure effects are not neglected in welding simulation.
3- A complete and reliable expert software for welding simulation is produced to be able to eliminate verification experiments (Hole-Drilling or the other stress measurement methods).

## References


1. Macherauch E, Kloss KH, Proc international conference on residual stresses, Gramish-Partenkirchen (FRG), 1986, pp.3–26.
2. Grayli N, Shyne JC, Effect of microstructure and prior austenite grain size on acoustic velocity and attenuation in steel, Rev Prog NDE, 1985, vol.4B, pp. 927–936.
3. Herzer R, Schneider E, Instrument for the automated ultrasonic time-of-flight measurement a tool for materials characterization, Springer, 1989, pp. 673–680.
4. Palanchamy P, Joseph A, Jayakumar T, Ultrasonic velocity measurements for estimation of grain size in austenitic stainless steel, NDT E Int, 1995, vol. 28, no. 3, pp. 179–185.
5. Papadakis EP, Physical acoustics and microstructure of iron alloys, Int Mater Rev, 1984, vol. 29, pp. 1–24.
6. Hakan Gür C, Orkun Tuncer B, Nondestructive investigation of the effect of quenching and tempering on medium-carbon low alloy steels, Int J Microstruct Mater Prop, 2005, vol. 1, no. 1, pp. 51–60.
7. Ploix MA, El Guerjouma R, Moysan J, Corneloup G, Chassignole B, Acoustical characterization of austenitic stainless-steel welds for experimental and modeling, NDT. J Soc Adv Sci, 2005, vol. 17, no. 1, pp. 76–81.
8. Spies M, Schneider E, Non-destructive analysis of texture in rolled sheets by ultrasonic techniques, Text Microstruct , 1990, vol. 12, pp. 219–213.
9. Johnson GC, Acoustoelastic response of a polycrystalline aggregate with orthotropic texture, J Appl Mech, 1985, vol. 52, pp. 659–663.
10. Sayers CM, Ultrasonic velocities in anisotropic polycrystalline aggregates, J Phys D Appl Phys, 1982, vol. 15, pp. 2157–2167.
11. Hakan Gür C, Çam İ, Comparison of magnetic Barkhausen noise and ultrasonic velocity measurements for microstructure evaluation of SAE 1040 and SAE 4140 steels, Materials Charact, 2007, vol. 58, no. 5, pp. 447–454C.
12. Nam YH, Kim YI, Nahm SH, Evaluation of fracture appearance transition temperature to forged 3Cr-1Mo-0.25 V steel using ultrasonic characteristics, Mater Lett., 2006, vol. 60, pp. 3577–3581.
13. Cantrell JH, Salama K, Acoustoelastic characterization of materials, Int Mater Rev, 1991, vol. 36, pp. 125–145.
14. Salama K, Relationship between temperature dependence of ultrasonic velocity and stress, Quantitative non-destructive evaluation, 1985, pp. 1109–1119
15. Mohbacher H, Schneider E, Goebbels K, Temperature dependence of third-order elastic constants, Proc 9th international conference on experimental mechanics, 1990, vol. 3, pp. 1189–1197.
16. Crecraft DI, The measurement of applied and residual stresses in metals using ultrasonic waves, J Sound Vib., 1967, vol. 5, no. 1, pp. 173–192.
17. Lhémery A, Calmon P, Chatillon S, Gengembre N, Modeling of ultrasonic fields radiated by contact transducer in a component of irregular surface, Ultrasonics, 2002, vol. 40, pp. 231–236.

18. A. P. Chakravati, L. M. Malik, and J. A. Goldak, Prediction of Distortion and Residual Stresses in Panel Welds, Computer modelling of fabrication processes and constitutive behaviour of metals, 1986, pp. 547–561.
19. J. Goldak and M. Bibby, Computational Thermal Analysis of Welds, Modeling of Casting and Welding Processes, 1988, vol. 4 , pp. 153–166.
20. H. Hibbitt and P. V. Marcal, A Numerical, Thermo-Mechanical Model for the Welding and Subsequent Loading of a Fabricated Structure, Computers & Structures, 1973, vol. 3, pp. 1145-1174.
21. J. H. Argyris, J. Szimmat, and K. J. Willam, Computational Aspects of Welding Stress Analysis, Computer Methods in Applied Mechanics and Engineering, 1982, vol. 33, pp. 635–666.
22. E. F. Rybicki, D. W. Schmueser, R. B. Stonesifer, J. J. Groom, and H. W. Mishler, A Finite-Element Model for Residual Stresses and Deflections in Girth-Butt Welded Pipes, Journal of Pressure Vessel Technology, 1978, vol. 100, pp. 256–262.
23. V.J Papazoglou and K. Masubuchi, Numerical Analysis of Thermal Stresses during Welding including Phase Transformation Effects, Journal of Pressure Vessel Technology, 1982, vol. 104, pp. 198–203.
24. Y. Ueda KH. Murakawa N. X. Ma and H. Maeda, FEM Analysis of 3-D Welding Residual Stresses and Angular Distortion in T-type Fillet Welds, Transactions of JWRI, 1995, vol. 24, no. 2, pp. 115–122.
25. Egle, D.M., Bray, D.E., Measurement of acoustoelastic and third order elastic constants for rail steel, J. Acoust. Soc. Am, 1976, vol. 60, no. 3, pp. 741–744.
26. Bray, D.E., Stanley, R.K., Nondestructive Evaluation. CRC Press, Boca Raton, FL revised edition(1997).
27. Brekhovskii, L.M., Waves in Layered Media, Academic Press, 1960, vol. 1.
28. Basatskaya, L.V., Ermolov, I.N., Theoretical study of ultrasonic longitudinal subsurface waves in solid media, 1980.
29. Junghans, P., Bray, D.E., Beam characteristics of high angle longitudinal wave probes, In: R.N. Pangbom, 1991.
30. Langenberg K.J., Fellenger P., Marklein R., On the nature of the so-called subsurface longitudinal wave and/or the surface longitudinal 'creeping' wave, Res. Nondest. Eval., 1990, vol. 2, pp. 59–81.
31. Bray, Don E. and Tang, Wei, Evaluation of Stress Gradients in Steel Plates and Bars with the $L_{CR}$ Ultrasonic Wave, Nuclear Engineering and Design, 2001, vol. 207, pp. 231-240.
32. J.Goldak, M.Akhlaghi, Computational Welding Mechanics, Springer, 2005.
33. Lindgren LE, Finite element modelling and simulation of welding part 2: improved material modeling, J Thermal Stress, 2001, vol. 24, pp. 195–231.
34. Lindgren LE, Hedblom R, Modelling of addition of filler material in large deformation analysis of multipass welding, Commun Numer Methods Eng, 2001, vol. 17, pp. 647–57.
35. P. Chang, T. Teng, Numerical and experimental investigations on the residual stresses of the butt-welded joints, Computational Materials Science, 2004, vol. 29, pp. 511–522.
36. A. Schaeffler, Constitution diagram for stainless steel weld metal, Metal Progress, 1949, pp. 680-680.
37. Lindgren LE, Finite Element Modelling and Simulation of Welding Part 1: Increased complexity, J Thermal Stress, 2001, vol. 24, pp. 141–92.
38. Deng D, Murakawa H, Numerical simulation of temperature field and residual stress in multi-pass welds in stainless steel pipe and comparison with experimental measurements, Computational Materials Science, 2006, vol. 37, no. 3, pp. 269-277.
39. H. Qozam, S. Chaki, G. Bourse, C. Robin, H. Walaszek, P. Bouteille, Microstructure Effect on the $L_{CR}$ Elastic Wave for Welding Residual Stress Measurement, Experimental Mechanics, 2010, vol. 50, pp. 179–185.

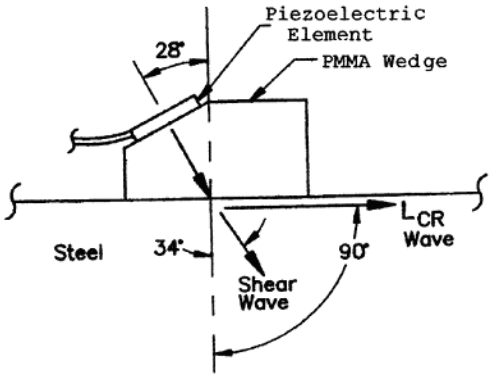


**Fig. 1.** $L_{CR}$ **probe for PMMA(plexiglas) wedge on steel[31]**

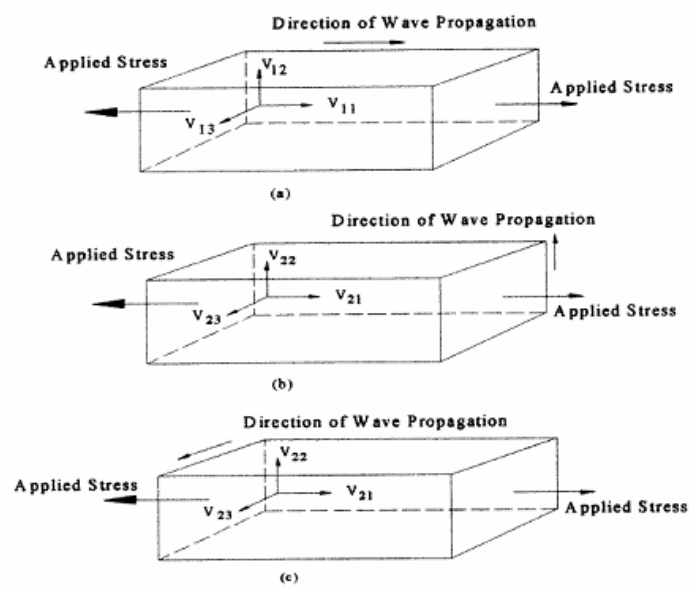


**Fig. 2. Velocity of plane wave and stress field in orthogonal directions[31]**

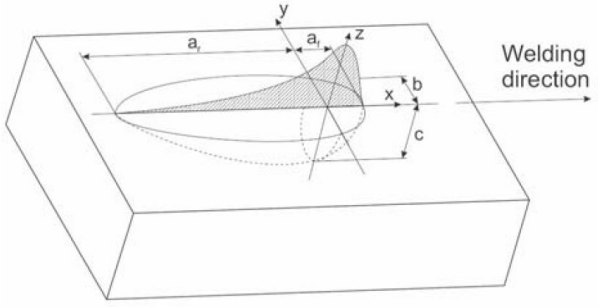


**Fig. 3 Double ellipsoid heat source configuration. [32]**

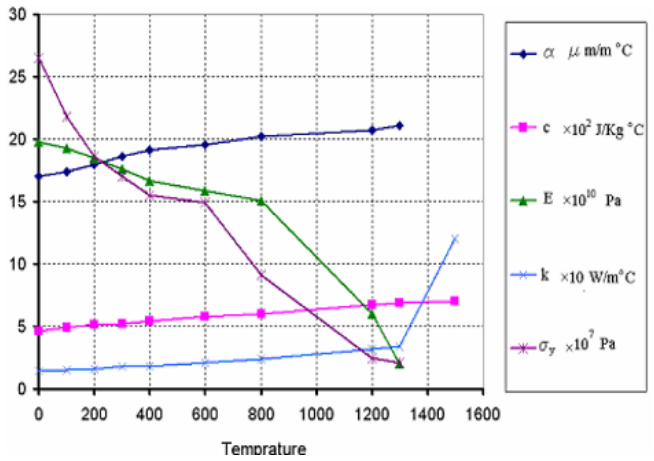


**Fig. 4 Material properties for 304 stainless steel used in this study [34]**

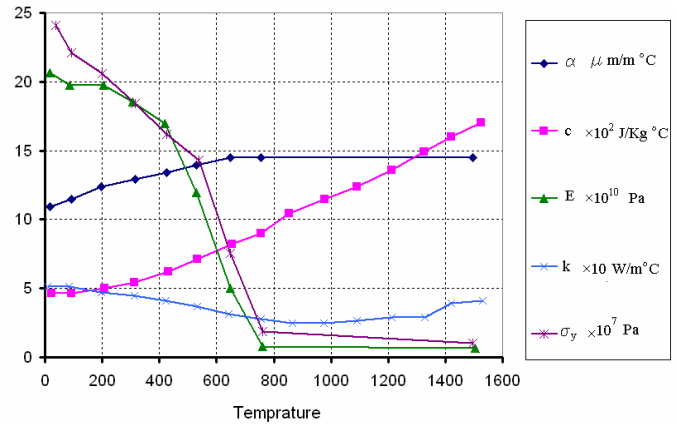


**Fig. 5 Material properties for A106-B carbon steel used in this study[35]**

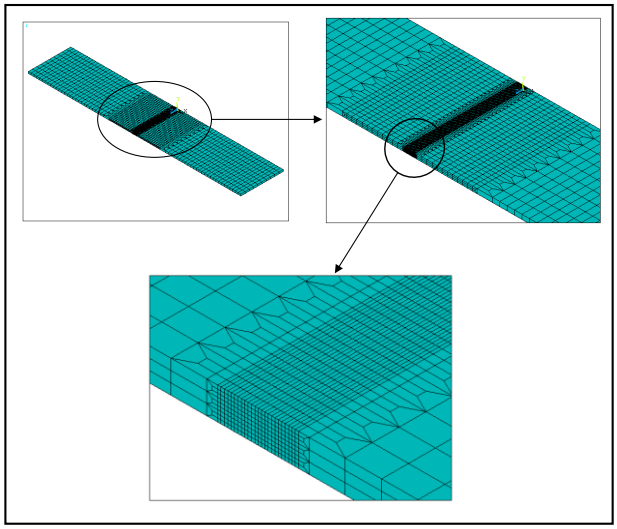

**Fig. 6 Basic FE model of dissimilar joint**

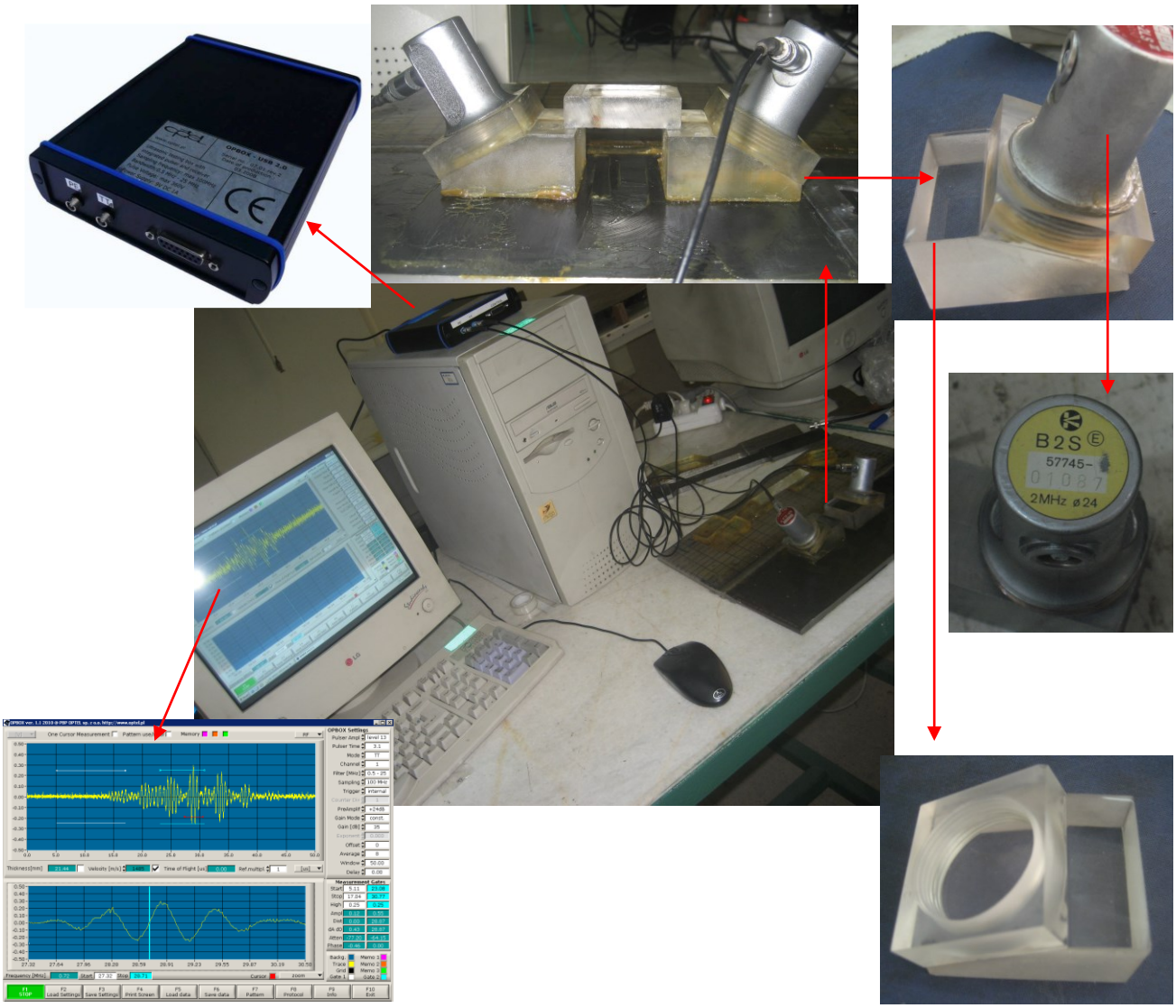


**Fig. 7. Measurement Devices**

**Fig. 8. Tensile test to evaluate acoustoelastic constant( $L_{11}$ ) in two different extracted samples**

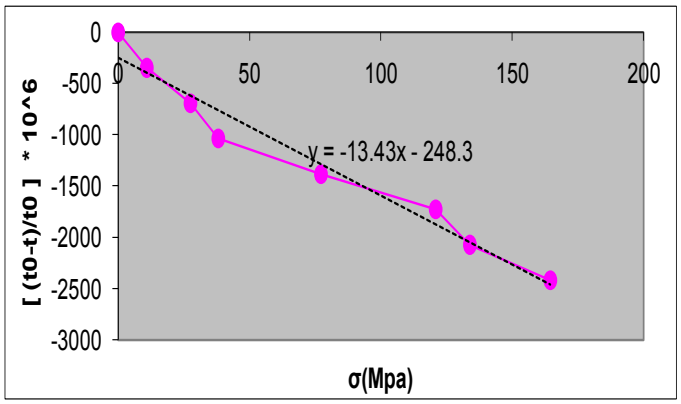


**Fig. 9. Result of Tensile test on carbon steel sample to evaluate acoustoelastic constant**

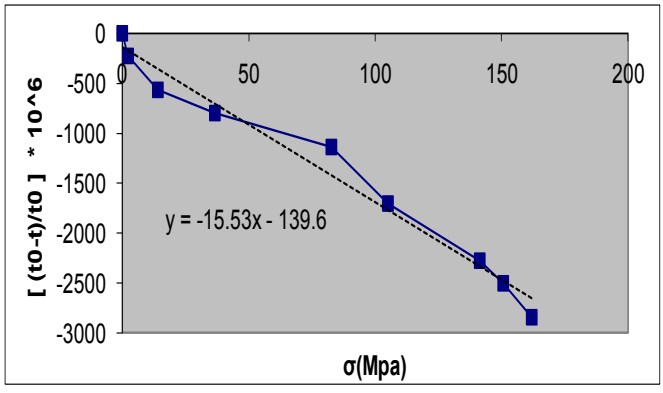


**Fig. 10. Result of Tensile test on stainless steel sample to evaluate acoustoelastic constant**

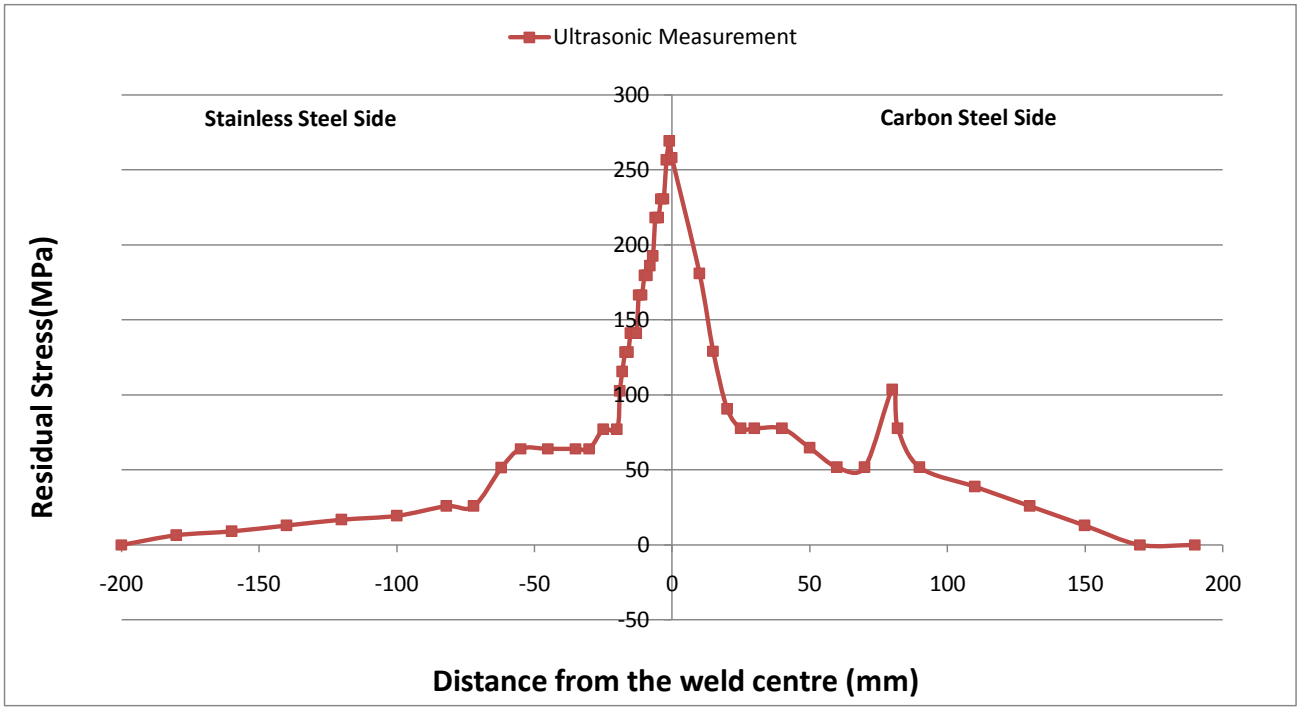


**Fig. 11. Ultrasonic stress measurement results on both side of the plates**

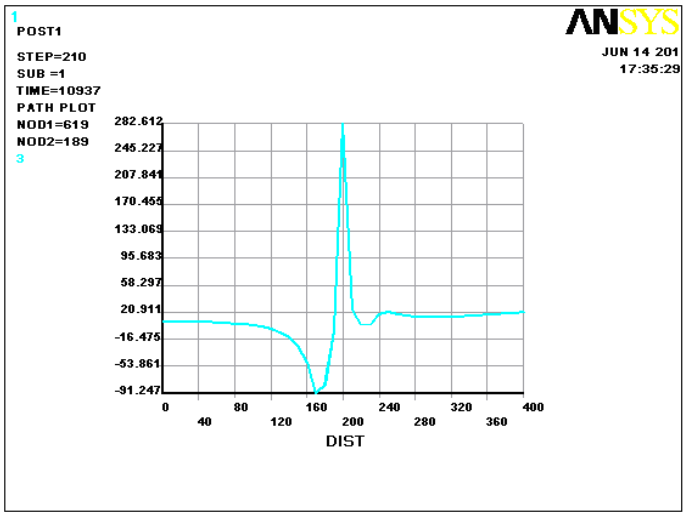


**Fig. 12. Residual stress evaluation using Ansys finite element software**

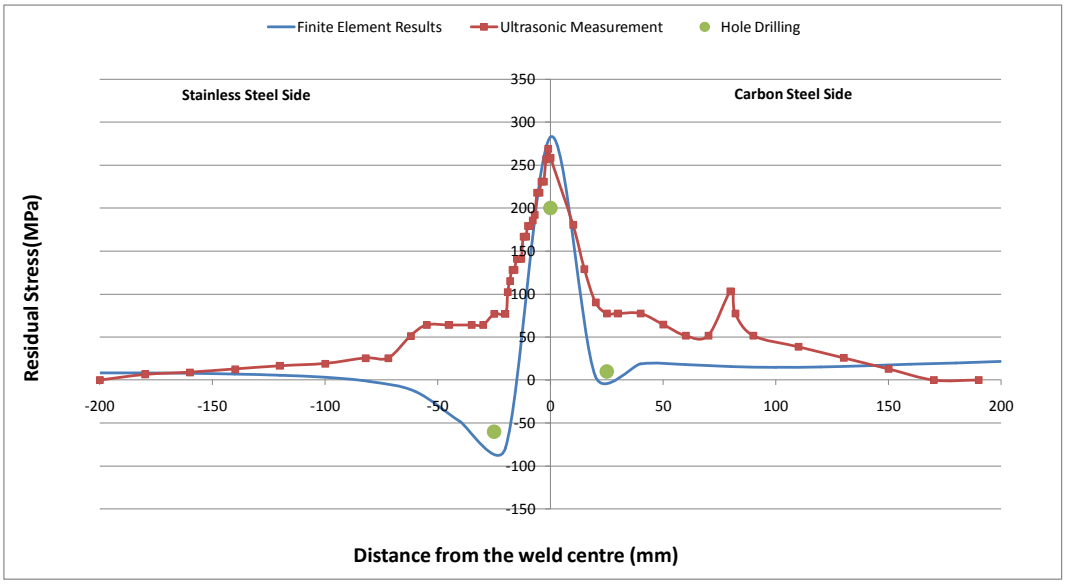


**Fig. 13. Comparison between the Ultrasonic, Finite Element and Hole-drilling stress measurement**